WebLog Journal of Materials Science and Engineering

Research Article

Published: 31 Jul, 2026

The Influence of Absorption on the Amplitudes of Emission Lines in Whispering Gallery Modes of a Spherical Microresonator with a Luminescent Shell

Alexander A. Dukin*

Researcher, Ioffe Institute, 26 Politekhnicheskaya, St. Petersburg, 194021, Russia

WebLog Open Access Publications

Article ID : wjmse.2026.g3102

Author : Dr. Alexander A. Dukin, Ph.D.

Abstract

The influence of absorption in the shell material on the amplitudes of lines of the TE and TM polarized whispering gallery modes (WGMs) in the emission spectrum of a microresonator structure consisting of a spherical core covered with a luminescent shell with a refractive index greater than that of the core was investigated. The luminescence spectra, radial field distribution and WGM parameters were calculated using the spherical wave transfer matrix method. It is shown that, for different shell thicknesses, the amplitudes of the peaks associated with radiation in WGMs of different polarizations (TE and TM) depend differently on the absorption coefficient: the amplitude of the TE mode radiation peak can be many times greater or many times less than the amplitude of the TM mode radiation peak.

Keywords: Spherical Microresonator; High-Refractive Index Luminescent Shell; Whispering Gallery Modes; Emission Line Amplitude; Absorption

OPEN ACCESS

Correspondence:

Dr. Alexander A. Dukin, Ph.D., Researcher, Ioffe Institute, 26 Politekhnicheskaya, St. Petersburg, 194021, Russia, Tel: +7 (812) 297-22-45;

E-mail: doukine@yandex.ru

Received Date: *14 Jun 2026*

Accepted Date: *29 Jul 2026*

Published Date: *31 Jul 2026*

Citation:

Alexander A. Dukin. The Influence of Absorption on the Amplitudes of Emission Lines in Whispering Gallery Modes of a Spherical Microresonator with a Luminescent Shell. WebLog J Materials Sci Eng. wjmse.2026.g3102. https://doi.org/10.5281/zenodo.21845507

Introduction

Spherical optical microresonators (MRs) with whispering gallery modes (WGMs) have attracted much attention in various fields of optics [1-4]. Their unique optical properties are due to whispering gallery modes - eigenmodes of the electromagnetic field of a spherical resonator that have a large angular momentum. WGMs have a high-quality factor, small effective volume and high energy density. WGM-based MRs can be used to detect the refractive index of the environment, chemicals, biological substances, pressure, temperature, to create microlasers with a low generation threshold, in optical communication and information processing systems, in quantum and nonlinear optics [5-9].

Small diameter MRs are attracting great interest due to their potential use as biological detectors for insertion into cells, body tissues, vessels, etc. Reducing the diameter of the MR and increasing the refractive index of the MR material allows for increasing the sensitivity of the sensor [10]. The use of luminescent MRs as sensors allows for remote excitation and detection of an optical signal through the photoluminescence (PL) spectra of the MRs. This avoids the difficulties associated with high-precision coupling of MR with waveguides, prisms, etc., which is difficult to achieve within a biological environment. Light-emitting MRs can be obtained by depositing a shell of luminescent material on a spherical transparent core. In the emission spectrum of the MR in WGMs there are two superimposed combs of narrow peaks, one of which corresponds to the emission in WGM with TE polarization, and the other to the emission in WGM with TM polarization. Each pair of adjacent peaks corresponds to radiation in WGMs with the same polar (l) and radial (q) mode numbers, but with different TE and TM polarizations. In an experiment, the task of interpreting and analyzing the obtained spectra often arises. From the PL spectrum, the wavelengths, quality factors, and amplitudes of the peaks corresponding to the radiation in the WGM are determined. Typically, the amplitude of the TE-polarized peak is larger (often approximately 1.5-2 times) than the amplitude of the TM-polarized peak with the same mode numbers. The amplitude of the peaks can be affected by many factors, including absorption in the shell material.

The aim of this work is a study of the influence of absorption in the shell material on the amplitudes of emission peaks in WGMs with different polarizations in the luminescence spectra of a microresonator structure consisting of a spherical optically transparent core of small diameter (3.5 µm) covered with an absorbing luminescent shell with a refractive index greater than the refractive index of the core.

Method for Calculating Luminescence Spectra

WGMs are described by spherical waves, which are characterized by three numbers: the polar mode number l ($l \geq 1$), the azimuthal mode number m ($m = l$ or m close to l), the radial mode number q ($q \geq 1$) and two polarizations (TE and TM). With TE polarization, the electric field vector is parallel to the MR surface; with TM polarization, the electric field vector is almost perpendicular to the MR surface. Further, WGMs will be designated as TE^q_l or TM^q_l, where TE and TM are WGM polarizations, q and l are the corresponding mode numbers. The emission spectra of the shell, the radial field distribution and the WGM parameters (wavelength, quality factor) were calculated using the expansion of the electromagnetic wave field in the basis of vector spherical harmonics and the method of spherical wave transfer matrices [11]. The calculated profiles of the radial distribution of the WGM field are normalized so that at the maximum the amplitude of the electric field strength is equal to 1.

The Microresonator Structure Under Study

The emission spectra of a MR structure with the following parameters were studied: core diameter 3.5 µm, refractive index of the core n_{co} = 1.46, refractive index of the radiating shell n_s = 2.25, shell thickness: 10, 80, 500 nm. This core refractive index corresponds to the refractive index of amorphous SiO_2. The refractive index of the shell corresponds to the refractive index of SiC. MR structures with such parameters (core diameter, refractive indices of the core and shell) were obtained earlier [12, 13]. The absorption in the shell material is determined by the imaginary part of the permittivity of the shell material $\mathrm{Im}\varepsilon_s$.

The emission spectrum of the luminescent shell consists of pairs of narrow peaks corresponding to the emission in WGMs with the same mode numbers l and q = 1, but with different polarizations TE and TM [11]. For the analysis, the TE^1_{32} and TM^1_{32} modes with amplitudes A_{TE} and A_{TM} and quality factors Q^{TE} and Q^{TM}, respectively, were used. Structures with a shell thickness of 10, 80 and 500 nm are considered, which correspond to cases where the optical thickness of the shell is much smaller, comparable or greater than the wavelengths of these modes. The dependence of the amplitudes of the TE^1_{32} and TM^1_{32} peaks on the imaginary part of the permittivity of the shell material was studied.

Results and Discussion

The probability of spontaneous emission (and according to the electrodynamic reciprocity principle, the probability of photon absorption) in a WGM inside a spherical microresonator Γ_{cav} compared to the case of emission (absorption) in free space Γ_{free} increases due to the Purcell effect by a factor of:

$$\frac{\Gamma_{cav}}{\Gamma_{free}} = \frac{3Q_{rad}\left(\lambda/n\right)^3}{4\pi^2 V_{eff}} \cdot \frac{\left|\mathbf{d}\cdot\mathbf{E}(\mathbf{r}_e)\right|^2}{\left|\mathbf{d}\right|^2} \quad (1)$$

where Q_{rad} is the radiative quality factor of the mode, V_{eff} is the effective volume of the mode, λ is the wavelength of the mode in vacuum, n is the refractive index of the substance inside the resonator, $\mathbf{d}$ is the transition dipole moment, $\mathbf{E}(\mathbf{r}_e)$ is the electric field of the mode, which is normalized so that at the maximum it is equal to 1, $\mathbf{r}_e$ is the position of the emitting (absorbing) dipole inside the resonator [14]. Thus, inside the resonator, the probability of absorption of a photon at the frequency of the resonant mode, compared to the case of free space, increases proportionally to Q_{rad} and the square of the electric field strength of the mode at the location of the dipole. Since the probability of photon absorption is directly proportional to Q_{rad}, modes with larger Q_{rad} are much more sensitive to absorption in the material in which the WGM propagates than modes with smaller Q_{rad}.

The total quality factor of WGMs (Q_{tot}) in real MRs is contributed by many mechanisms, such as radiation escape through the MR boundary (radiative losses, Q_{rad}), absorption in the resonator material, scattering by surface irregularities, etc. In our calculation we will only take into account the losses associated with radiation escape and absorption in the shell. The total quality factor will be determined by both the quality factor associated with radiative losses (Q_{rad}), and the quality factor associated with absorption in the shell material (Q_{abs}): $Q_{tot}^{-1} = Q_{rad}^{-1} + Q_{abs}^{-1}$. Q_{rad} is independent of $\mathrm{Im}\varepsilon_s$. Q_{abs} is infinitely large at zero absorption and decreases with increasing $\mathrm{Im}\varepsilon_s$. In the case when radiative losses are much greater than absorption losses: $Q_{rad}^{-1} \gg Q_{abs}^{-1}$, then $Q_{tot} \approx Q_{rad}$, Q_{tot} is constant and does not depend on $\mathrm{Im}\varepsilon_s$. In the case when the absorption losses are much greater than the radiation losses: $Q_{abs}^{-1} \gg Q_{rad}^{-1}$ then $Q_{tot} \approx Q_{abs}$, Q_{tot} depends on $\mathrm{Im}\varepsilon_s$ in the same way as Q_{abs}, i.e. it decreases with increasing $\mathrm{Im}\varepsilon_s$. As $\mathrm{Im}\varepsilon_s$ increases, the absorption losses increase (Q_{abs} decreases), as a result, at a certain threshold value of $\mathrm{Im}\varepsilon_s$, when Q_{abs} becomes approximately equal to Q_{rad}, the total quality factor begins to decrease with increasing $\mathrm{Im}\varepsilon_s$. As a consequence, from this threshold value $\mathrm{Im}\varepsilon_s$ the amplitude of the peak in the emission spectrum begins to decrease due to the increase in absorption losses in the shell material.

Figure 1 and Figure 2 show: the calculated distribution of the square of the modulus of the normalized electric field strength, the distribution of the normalized effective potential U_{eff} / E of the TE^1_{32} and TM^1_{32} modes along the radial coordinate, the dependence of the amplitudes of the radiation peaks A_{TE}, A_{TM} of these modes and their

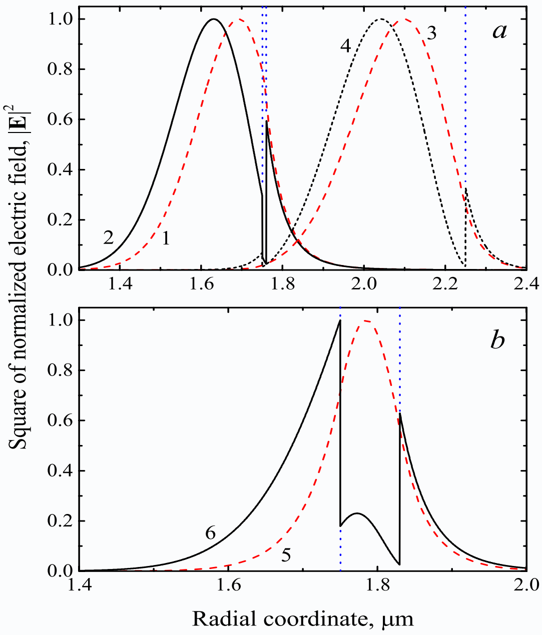

Figure 1: Distributions of the squared modulus of the electric field strength along the radial coordinate for the whispering gallery modes TE^1_{32} (red dashed lines 1, 3, 5) and TM^1_{32} (black lines 2, 4, 6), for three different shell thicknesses of 10 nm (*a*, lines 1, 2), 500 nm (*a*, lines 3, 4), 80 nm (*b*, lines 5, 6). The vertical dotted lines indicate the boundaries of the shell with the core and the external environment. The microresonator parameters are given in the text of the paper.

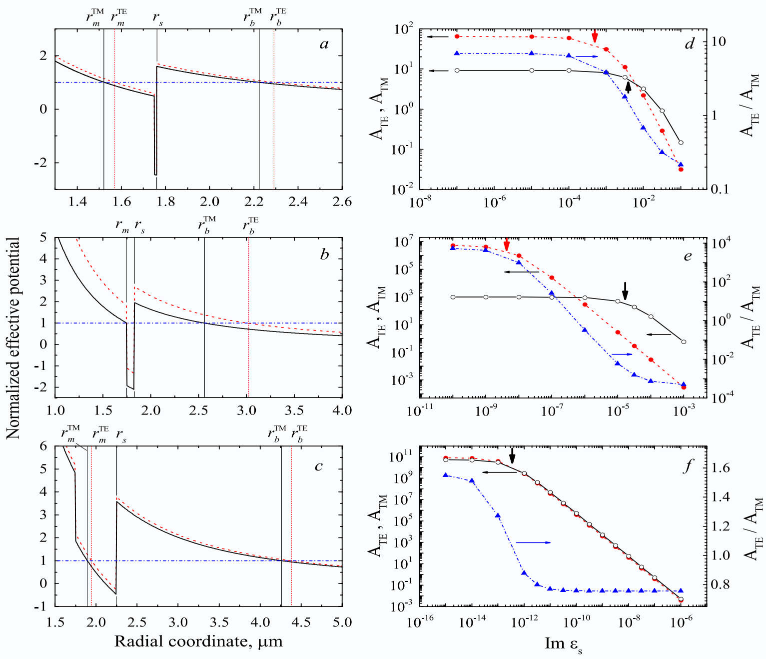

Figure 2: Distributions of the normalized effective potential U_{eff} / E (*a*, *b*, *c*) along the radial coordinate, the dependence of the peak amplitudes (A_{TE}, A_{TM} – red dashed and black solid lines, respectively) and the ratio of the amplitudes of these peaks (A_{TE} / A_{TM} - blue dashed-dotted line) on the imaginary part of the permittivity of the shell material Imε_s (*d*, *e*, *f*), for the whispering gallery modes TE^1_{32} (red dashed line) and TM^1_{32} (black solid line), for three different shell thicknesses of 10 nm (*a*, *d*), 80 nm (*b*, *e*), 500 nm (*c*, *f*). In the figures of the effective potential (*a*, *b*, *c*), the vertical thin lines show the boundaries of the potential well and the potential barrier for the TE mode (r_m^{TE} and r_b^{TE} – red dashed lines) and the TM mode (r_m^{TM} and r_b^{TM} – black solid lines), as well as the boundary of the shell with the external environment (r_s). The energy level in the normalized effective potential U_{eff} / E is shown by a horizontal blue dashed-dotted line at level 1. The vertical bold arrows (red and black for TE^1_{32} and TM^1_{32} modes, respectively) indicate the Imε_s threshold values at which the A_{TE} and A_{TM} peak amplitudes begin to decrease with increasing Imε_s (*d*, *e*, *f*). In *f*, these two vertical arrows coincide. The parameters of the microresonator are given in the text of the paper.

ratio A_{TE} / A_{TM} on Imε_s. The calculation was performed for three values of shell thickness (10 nm, 80 nm, 500 nm) with $n_s = 2.25$.

The equation for the radial dependence of the electric field of the mode corresponds to the Schrödinger equation for one-dimensional motion of a particle in an effective potential:

$$U_{eff} = E\left([1-n(r)^2]+\frac{l(l+1)}{r^2k_0^2}\right) \qquad (2)$$

where *n(r)* is the refractive index depending on the radial coordinate, *r* is the radial coordinate, k_0 is the wave vector in vacuum ($k_0 = 2\pi/\lambda$), λ is the wavelength of the mode in vacuum, *l* is the polar mode number, $E = \hbar^2 k_0^2/2M = \hbar\omega$ is the energy, $M = \hbar\omega/2c^2$ is the mass [4]. This potential depends on the wavelength of the mode and is therefore different for the TE^1_{32} and TM^1_{32} modes. It is formed by the centrifugal potential (the term $l(l+1)\lambda^2/r^2(2\pi)^2$) and the refractive index, which depends on the radial coordinate (the term $[1-n(r)^2]$). The effective potential has the form of a classical potential well, in which the photon moves between turning points r_m and r_s (Figure 2 *a*, *b*, *c*). Thus, WGMs are characterized by the fact that they are located in a potential well formed by the centrifugal potential from the core and experiencing a potential jump at the boundary with the external environment. The exit from this potential well is closed by a triangular-shaped potential barrier, which is located in the region $r_s < r < r_b$. The probability of tunneling through this barrier determines the radiative quality factor of the mode. Since the effective potential depends on the square of the mode wavelength, the width and height of this potential barrier differ for TE^1_{32} and TM^1_{32} modes. The radiative quality factor for TE^1_{32} and TM^1_{32} modes is for a thickness of 10 nm: $Q_{rad}^{TE} = 24653$, $Q_{rad}^{TM} = 15969$; for a thickness of 80 nm: $Q_{rad}^{TE} = 8.5704 \cdot 10^8$, $Q_{rad}^{TM} = 617710$; for a thickness of 500 nm: $Q_{rad}^{TE} = 2.3351 \cdot 10^{13}$, $Q_{rad}^{TM} = 1.6524 \cdot 10^{13}$. A shell with a refractive index greater than the refractive index of the core creates an additional potential well formed by jumps in the refractive index at the boundaries of the shell (a dip in the graph of the effective potential, Figure 2, *a*, *b*, *c*).

For the TE^1_{32} mode, the radial field distribution graphs represent a continuous curve with one broad maximum (Figure 1). For the TM^1_{32} mode, the graphs show two jumps at the shell boundaries, which arise due to the boundary conditions for the radial component of the electric field at the interface between two media with different permittivities (Figure 1). The selected shell thicknesses correspond to three different cases of radial distribution of the field of the studied modes in the shell: when almost the entire WGM field is in the core (10 nm, Figure 1*a*), when a significant part of the WGM field is in both the core and the shell (80 nm, Figure 1*b*), when almost the entire WGM field is in the shell (500 nm, Figure 1*a*).

For all three thicknesses, there is a region of small values of Imε_s (Figure 2, *d*, *e*, *f*), in which the amplitudes of both peaks are almost constant - this corresponds to the case when the absorption losses are much less than the radiation losses ($Q_{abs}^{-1} \ll Q_{rad}^{-1}$), the total quality factor is determined by Q_{rad}, and is approximately equal to it. Then, with an increase in Imε_s, starting from a certain threshold value of Imε_s (at which $Q_{abs} \approx Q_{rad}$, it is approximately indicated by vertical arrows in Figure 2, *d*, *e*, *f*), absorption losses become equal and then much greater than radiation losses ($Q_{abs}^{-1} \gg Q_{rad}^{-1}$), and the total quality factor is determined by Q_{abs}. Starting from this threshold value, the amplitudes of A_{TE}, A_{TM} begin to decrease with increasing Imε_s - approximately linearly on a double logarithmic scale. In the case of a thick shell, they decrease synchronously and in parallel (Figure 2, *f*, the threshold values for TE^1_{32} and TM^1_{32} are very close). In the case of a thin shell (Fig. 2, *d*) and intermediate thickness (Figure 2, *e*), the threshold values differ significantly: first, the amplitude of the TE^1_{32} mode begins to decrease (since it has a larger Q_{rad}), and then, with a larger value of $Im\varepsilon_s$, the amplitude of the TM^1_{32} mode. Moreover, the difference between the threshold values $Im\varepsilon_s$ for TE^1_{32} and TM^1_{32} for a thickness of 80 nm is much greater than for a thickness of 10 nm (Figure 2, *d*, *e*). Accordingly, as $Im\varepsilon_s$ increases, the A_{TE} / A_{TM} amplitude ratio begins to decrease. For a thick shell, it decreases by only a factor of 2 (Figure 2, *f*); for a very thin shell, it decreases by a factor of 32 (Figure 2, *d*); and for intermediate thicknesses, it decreases by several orders of magnitude (Figure 2, *e*). Thus, depending on the thickness of the shell and the absorption coefficient, the amplitude of the TE mode radiation peak can be many times greater or many times less than the amplitude of the TM mode radiation peak. This different behavior is due to the different distribution of the WGM field relative to the shell in which absorption occurs and the different radiative quality factors of TE^1_{32} and TM^1_{32} modes (since both factors contribute to the probability of absorption of a photon in the WGM: Q_{rad} and the magnitude of the electric field strength of the WGM at the point where the absorber is located – formula (1)). As a result, the threshold values of $Im\varepsilon_s$ at which the peak amplitude begins to decrease with increasing absorption differ for TE^1_{32} and TM^1_{32} modes.

At a thickness of 500 nm, the radiative quality factors of both modes are close ($Q^{TE}_{rad}/Q^{TM}_{rad} = 1.4$) and in the shell region the electric field profiles of the TE^1_{32} and TM^1_{32} modes differ insignificantly (Figure 1, *a*, lines 3, 4). This results in approximately the same magnitude of absorption losses for both TE^1_{32} and TM^1_{32} modes, and, accordingly, an almost identical threshold value of $Im\varepsilon_s$, an almost synchronous decrease in peak amplitudes, and, as a consequence, a relatively small decrease in A_{TE} / A_{TM} with increasing $Im\varepsilon_s$.

At a thickness of 10 nm, the radiative quality factors of both modes are close ($Q^{TE}_{rad}/Q^{TM}_{rad} = 1.5$) but in the shell region the electric field strength of the TM^1_{32} mode is many times less than the electric field strength of the TE^1_{32} mode (due to the jumps in the refractive index at the boundary for the TM^1_{32} mode there is a sharp dip in the mode field profile, Figure 1, *a*, lines 1, 2). This causes lower losses due to absorption for the TM^1_{32} mode compared to the TE^1_{32} mode, and as a consequence, a different threshold value of $Im\varepsilon_s$ (a difference of ~8 times) and an asynchronous decrease in amplitudes with an increase in $Im\varepsilon_s$. The latter results in a greater reduction in A_{TE} / A_{TM} with increasing $Im\varepsilon_s$.

At a thickness of 80 nm, the radiative quality factor of the TE^1_{32} mode is 3 orders of magnitude greater than the radiative quality factor of the TM^1_{32} mode ($Q^{TE}_{rad}/Q^{TM}_{rad} = 1387$). As in the case of a thickness of 10 nm, in the shell region the electric field strength of the TE^1_{32} mode is several times greater than the electric field strength of the TM^1_{32} mode (due to jumps in the refractive index at the shell boundary, Figure 1, *b*). Both of these factors result in a much higher probability of photon absorption and much higher absorption losses for the TE^1_{32} mode compared to the TM^1_{32} mode. As a result, the threshold values of $Im\varepsilon_s$ for TE^1_{32} and TM^1_{32} differ very significantly (by a factor of ~4760) and this leads to a very significant decrease in A_{TE} / A_{TM} with increasing $Im\varepsilon_s$. Accordingly, depending on the absorption value in the shell material, it is possible to obtain radiation predominantly in the TE or TM polarized WGMs.

The significantly different radiative quality factors of TE^1_{32} and TM^1_{32} at a shell thickness of 80 nm are due to the different mechanisms of confinement of these modes at this thickness. At thicknesses of 10 and 500 nm (Figure 2, a, c), both modes are limited by the centrifugal potential in the core (for 10 nm) or shell (for 500 nm), and by the potential jump at the interface with the external medium. Thus, both modes propagate as whispering gallery modes in the core (for 10 nm) or shell (for 500 nm). This is also true for the TM^1_{32} mode at a thickness of 80 nm (Figure 2, *b*). However, at a thickness of 80 nm, the TE^1_{32} mode is limited on both sides by potential jumps at the outer and inner boundaries of the shell (Figure 2, *b*). Consequently, it propagates as a waveguide mode within the shell. This leads to a large difference in wavelength between TE^1_{32} and TM^1_{32} modes. Moreover, for the TE^1_{32} mode (compared to the TM^1_{32} mode) there is a significantly higher and wider potential barrier (Figure 2, *b*), caused by the greater centrifugal potential due to the longer wavelength of the mode (formula (2)). This results in much lower radiative losses associated with tunneling through this barrier, which leads to a higher (by 3 orders of magnitude) radiative quality factor for TE^1_{32} mode compared to TM^1_{32} mode. And this ultimately leads to a much larger range of change in the ratio of the amplitudes of the peaks of these modes: A_{TE} / A_{TM} with increasing $Im\varepsilon_s$.

Knowing the ratio of the amplitudes A_{TE} / A_{TM} from the experimental spectrum and using the calculated dependences of A_{TE} / A_{TM} on $Im\varepsilon_s$, one can in turn determine the value of the imaginary part of the permittivity in the shell material. This is possible provided that the remaining parameters of the structure (core diameter, shell thickness, refractive indices of the core and shell) are precisely known, that the WGMs are correctly identified in the PL spectrum (their mode numbers *l*, *q* are determined), and that all other broadening mechanisms except for radiation and absorption in the shell material can be neglected.

Conclusion

The paper considers the influence of absorption on the luminescence spectra in whispering gallery modes for core-shell microresonators. The microresonator structure consists of a spherical optically transparent dielectric core of small diameter (3.5 μm) surrounded by an absorbing luminescent shell with a refractive index greater than that of the core. The dependence of the ratio of peak amplitudes (A_{TE} / A_{TM}) corresponding to radiation in the TE^1_{32} and TM^1_{32} WGMs on the value of the absorption in the shell material was investigated.

It is shown that when the optical thickness of the shell is much smaller than the wavelength of the modes (the WGM field is localized predominantly in the core), the A_{TE} / A_{TM} ratio decreases monotonically with an increase in the imaginary part of the permittivity of the shell material, and the amplitude of the TE peak can be either several times greater or several times smaller than the amplitude of the TM peak.

When the optical thickness of the shell is greater than the wavelengths of the modes, the WGM field is localized almost entirely in the shell. In this case, the amplitudes of the peaks differ slightly, and their ratio (A_{TE} / A_{TM}) changes from 1.5 to 0.76 with an increase in the imaginary part of the permittivity of the shell material.

At some intermediate shell thicknesses (80 nm), when the optical thickness of the shell is several times smaller than the wavelength of the modes under consideration, the field of both modes is localized both in the shell region and in the core. In this case, the amplitude of the TE mode peaks can be several orders of magnitude greater or less than the amplitude of the TM mode peak with the same mode numbers, depending on the imaginary part of the permittivity of the shell material.

Funding

This work was supported by state assignment no. FFUG-2024-0017.

Conflict of Interest

The author declares that he has no conflict of interest.

References

1. Cai L, Pan J, Zhao Y, Wang J, Xiao S. Whispering Gallery Mode Optical Microresonators: Structures and Sensing Applications. Phys. Status Solidi A. 2020; V217 (6): 1900825. https://doi.org/10.1002/pssa.201900825

2. Righini G. C, Dumeige Y, Féron P, Ferrari M, Nunzi Conti G, Ristic D, Soria S. Whispering gallery mode microresonators: Fundamentals and applications. Nuovo Cimento. 2011; V34 (7): 435-488. http://doi.org/10.1393/ncr/i2011-10067-2

3. Ward J, Benson O. WGM microresonators: sensing, lasing and fundamental optics with microspheres. Laser Photonics Review. 2011; V5 (4): 553-570. http://doi.org/10.1002/lpor.201000025

4. Gorodetsky M. L. Opticheskie microrezonatory s gigantskoj dobrotnost'yu. Moskva, Russia: Fizmatlit 2011. (in Russian). https://www.rfbr.ru/library/books/1790/

5. Foreman M. R, Swaim J. D, Vollmer F. Whispering gallery mode sensors. Adv. Opt. Photon. 2015; V7 (2): 168-240. http://doi.org/10.1364/AOP.7.000168

6. Reynolds T, Riesen N, Meldrum A, Fan X, Hall J. M. M, Monro T. M, Francois A. Fluorescent and lasing whispering gallery mode microresonators for sensing applications. Laser Photonics Review. 2017; V11(2): 1600265. http://doi.org/10.1002/lpor.201600265

7. Righini G. C, Soria S. Biosensing by WGM Microspherical Resonators. Sensors. 2016; V16 (6): 905. http://doi.org/10.3390/s16060905

8. Jiang X, Qavi A. J, Huang S. H, Yang L. Whispering-Gallery Sensors. Matter, 2020; V3 (2): 371-392. http://doi.org/10.1016/J.MATT.2020.07.008

9. Venkatakrishnarao D, Mamonov E. A, Murzina T. V, Chandrasekar R. Advanced Organic and Polymer Whispering-Gallery-Mode Microresonators for Enhanced Nonlinear Optical Light. Advanced Optical Materials. 2018; V6: 1800343. http://doi.org/10.1002/adom.201800343

10. Reynolds T, Henderson M. R, Francois A, Riesen N, Hall J. M. M, Afshar S. V, Nicholls S. J, Monro T. M. Optimization of whispering gallery resonator design for biosensing applications. Optics Express. 2015; V23 (13): 17067-17076. http://doi.org/10.1364/OE.23.017067

11. Hall J. M. M, Reynolds T, Henderson M. R, Riesen N, Monro T. M, Afshar S. Unified theory of whispering gallery multilayer microspheres with single dipole or active layer sources. Optics Express. 2017; V25 (6): 6192-6214. http://doi.org/10.1364/OE.25.006192

12. Grudinkin S. A, Dontsov A. A, Feoktistov N. A, Baranov M. A, Bogdanov K. V, Averkiev N. S, Golubev V. G. Whispering gallery modes in a spherical microcavity with a photoluminescent shell. Semiconductors. 2015; V49 (10): 1369–1374. http://doi.org/10.1134/S1063782615100085

13. Grudinkin S. A, Feoktistov N. A, Trofimova E. Yu, Kurdyukov D. A, Bogdanov K. V, Baranov A. V, Fedorov A. V, Golubev V. G. Spherical microresonators with luminescent a-Si:C:H coating. Technical Physics Letters, 2013; V39 (4): 341–343. https://doi.org/10.1134/S1063785013040068

14. Confined Photon Systems: Fundamentals and Applications, ed. by Benisty H, Weisbuch C, Gérard J. M, Houdré R, Rarity J. Springer-Verlag, Berlin Heidelberg, 1999. http://doi.org/10.1007/BFb0104378